

# Ultrastructural changes in atherosclerotic plaques following the instillation of airborne particulate matter into the lungs of rabbits

Erin M Tranfield PhD, Stephan F van Eeden MD PhD, Kazuhiro Yatera MD, James C Hogg MD PhD, David C Walker PhD

EM Tranfield, SF van Eeden, K Yatera, JC Hogg, DC Walker. Ultrastructural changes in atherosclerotic plaques following the instillation of airborne particulate matter into the lungs of rabbits. *Can J Cardiol* 2010;26(7):e258-e269.

**BACKGROUND:** Epidemiological studies have established that cardiovascular events account for the greatest number of air pollution-related deaths. However, the underlying structural changes are still unknown.

**OBJECTIVE:** To investigate changes in the ultrastructure of atherosclerotic plaques in Watanabe heritable hyperlipidemic (WHHL) rabbits following the instillation of ambient particulate matter air pollution (particles smaller than 10 µm in diameter) into the lungs.

**METHODS:** WHHL rabbits (n=8) exposed to 5 mg of ambient particles (Environmental Health Centre – 1993 [EHC-93]; suspended in saline and instilled in the airway) twice per week for four weeks were compared with control WHHL rabbits (n=8) treated with saline alone.

**RESULTS:** All abdominal aortic plaques were examined using light and electron microscopy, which showed the following: increased accumulation of macrophage-derived foam cells immediately below the endothelial plaque surface (P=0.04); increased contact between these foam cells and the dense subendothelial extracellular matrix (P<0.005) with reduction (P<0.0001) and fragmentation (P<0.0001) of this matrix; and emigration of macrophage-derived foam cells from the plaques in exposed rabbits. In addition, immunohistochemistry verified the presence of type IV collagen in the thickened extracellular matrix material subtending the endothelium.

**CONCLUSIONS:** The ultrastructure of atherosclerotic plaques in EHC-93-instilled rabbits differed from the ultrastructure observed in rabbits that did not receive EHC-93. These ultrastructural differences are consistent with greater endothelial instability in the plaques of atherosclerosis-prone rabbits.

**Key Words:** Air pollution (PM<sub>10</sub>); Atherosclerosis; Electron microscopy; Watanabe heritable hyperlipidemic rabbits

Epidemiological studies have established a strong association between exposure to particulate air pollution (particles smaller than 10 µm in diameter; PM<sub>10</sub>) and cardiopulmonary morbidity and mortality (1-3). Cardiovascular events account for the greatest proportion of these adverse incidents (4,5), particularly in high-risk populations with a history of myocardial infarction (4,6) or chronic diabetes (7,8). The occurrence of myocardial infarctions (9), strokes (10), heart failure exacerbations (5), cardiac arrhythmias (11) and sudden deaths (12) increases within hours of the onset of an episode of elevated air pollution. In addition, PM<sub>10</sub> exposure has been associated with changes in blood pressure (13), plasma viscosity (14), arterial vasoconstriction (15), fibrinogen levels (16), interleukin (IL)-6 release (17), coagulation time (17), platelet activation (18), and early bone marrow release of neutrophilic polymorphonuclear leukocytes (19) and monocytes (20).

James Hogg iCAPTURE Research Centre, Providence Heart + Lung Institute, St Paul's Hospital; Department of Pathology and Laboratory Medicine, University of British Columbia, Vancouver, British Columbia

Correspondence and reprints: Dr David C Walker, UBC James Hogg Research Centre, Providence Heart + Lung Institute, St Paul's Hospital,

Room 166 – 1081 Burrard Street, Vancouver, British Columbia V6Z 1Y6. Telephone 604-806-8346, fax 604-806-8351, e-mail dwalker@mrl.ubc.ca  
Received for publication August 13, 2009. Accepted December 31, 2009

Les modifications ultrastructurelles des plaques athéroscléreuses après l'instillation de particules aéroportées dans les poumons de lapins

**HISTORIQUE :** Des études épidémiologiques ont établi que les événements cardiovasculaires expliquent la plupart des décès liés à la pollution de l'air. Cependant, on ne connaît toujours pas les modifications structurelles sous-jacentes.

**OBJECTIF :** Explorer les modifications de l'ultrastructure des plaques athéroscléreuses chez des lapins Watanabe ayant une hyperlipidémie à transmission héréditaire (WHLH) après l'instillation de particules d'air ambiant pollué (particules d'un diamètre inférieur à 10 µm) dans leurs poumons.

**MÉTHODOLOGIE :** Les lapins WHLH (n=8) exposés à 5 mg de particules d'air ambiant (*Environmental Health Centre – 1993 [EHC-93]*, suspendues dans une solution saline puis instillées dans les voies aériennes) deux fois par semaine pendant quatre semaines ont été comparés à des lapins WLHH (n=8) témoins traités avec une solution saline seulement.

**RÉSULTATS :** Les chercheurs ont examiné toutes les plaques aortiques abdominales au moyen des microscopies photonique et électronique qui ont révélé une accumulation accrue de cellules spumeuses dérivées des macrophages immédiatement sous la surface de la plaque endothéliale (P=0,04); un plus grand contact entre ces cellules spumeuses et la matrice extracellulaire subendothéliale dense (P<0,005), laquelle était à la fois réduite (P<0,0001) et fragmentée (P<0,0001) et la migration des cellules spumeuses dérivées des macrophages de la plaque chez les lapins exposés. De plus, l'immunohistochimie a corroboré la présence de collagène de type IV dans la matrice extracellulaire épaissie sous-tendant l'endothélium.

**CONCLUSIONS :** L'ultrastructure des plaques athéroscléreuses de lapins à qui on a instillé de l'EHC-93 différait de celle de lapins à qui on n'en avait pas instillé. Ces différences ultrastructurelles corroborent la plus grande instabilité endothéliale des plaques de lapins enclins à l'athérosclérose.

Atherosclerotic plaque disruption and thrombus formation underlie the pathogenesis of myocardial infarction, stroke and sudden death (21). Vulnerable plaques are characterized by a core of extracellular lipid and cellular debris that accounts for approximately 40% of the plaque volume (21,22). The fibrous cap covering the lipid core thins in association with the accumulation of macrophage-derived foam cells, a decrease in the smooth muscle cell (SMC) population and a reduction in collagen content (23,24). Plaques with this phenotype are vulnerable to rupture leading to occlusion of the lumen by thrombus formation or, potentially, distal thromboembolic events (21,23).

PM<sub>10</sub> exposure has been shown to produce both a local inflammatory response within the lungs and an acute-phase systemic inflammatory process characterized by an increase in circulating C-reactive protein (25) and a release of premature polymorphonuclear neutrophilic leukocytes (band cells) into the circulation (26).

Suwa et al (26) provided light microscopic evidence that PM<sub>10</sub> exposure leads to increased plaque size, lipid deposition and inflammatory cell recruitment into atherosclerotic plaques in Watanabe heritable hyperlipidemic (WHHL) rabbits. Sun et al (27,28) used an apolipoprotein E knockout (ApoE<sup>-/-</sup>) mouse model to show that long-term exposure to low concentrations of PM<sub>2.5</sub> (particles smaller than 2.5 µm in diameter) altered vasomotor tone, and increased tissue-factor expression, vascular inflammation and atherosclerotic burden in these animals. Research at the Lovelace Respiratory Research Institute (New Mexico, USA) in ApoE<sup>-/-</sup> mice has shown vascular remodelling and altered atherosclerotic plaque composition following PM<sub>10</sub> exposure and diesel emission exposure (29-31). The present study was designed to determine whether and how PM<sub>10</sub> exposure affected the architecture of existing atherosclerotic plaques and to determine whether the observed ultrastructure was consistent with the characteristics of a more vulnerable atherosclerotic plaque.

## METHODS

### Animals

These studies were approved by the Animal Experimentation Committee of the University of British Columbia (Vancouver, British Columbia). Female WHHL rabbits (n=16) (Covance Research Products Inc, USA) weighing a mean (± SD) of 3.5±0.4 kg were fed standard rabbit chow. Rabbits were sacrificed at 42 and 46 weeks of age at the completion of a four-week exposure protocol. The rabbits used in the present study were also used in other investigations to address monocyte release from the bone marrow (20) and monocyte recruitment into atherosclerotic plaques (32).

### Urban PM<sub>10</sub>

The urban PM<sub>10</sub> (ambient particulates) used in the present study, designated as Environmental Health Centre – 1993 (EHC-93), were obtained from Environment Canada; EHC-93 had been collected from the troposphere in Ottawa (Ontario) in 1993 using a single-pass, videon bag-house filtration system located at the Environmental Health Centre. The complete size distribution and composition of EHC-93 was described by Vincent et al (33) in 1997 and compared with eight other urban particulates. This size analysis of EHC-93 showed a mean diameter of 0.8±0.4 µm, with 99% of the number of particles less than 3.0 µm, which is similar to other urban particulate samples (33). The EHC-93 particles are aged and complex (ie, they contain both organic and inorganic components), and, relative to the other urban particulates, have high levels of many transition metals including chromium, manganese, nickel, vanadium and zinc (33) – many of which have exposure limits set by the WHO (34). It has been suggested that transition metals on the surface of airborne particles may have increased toxicity (35).

### Exposure protocol

The model used to test the hypothesis of the present study has been established in the James Hogg iCAPTURE Research Centre, Providence Heart + Lung Institute (Vancouver, British Columbia), and is well characterized with regard to both the local and the systemic response (20,26,32,36,37). Briefly, the experimental rabbits (n=8) were lightly anesthetized with 5% halothane while 5 mg of EHC-93, suspended in 1 mL of sterile saline, was deposited just above the larynx using a blunt curved needle twice per week for four weeks. A second group of eight similarly anesthetized rabbits that only had 1 mL of sterile saline injected above the larynx served as controls. Following the four-week exposure period, the rabbits were sacrificed with an overdose of sodium pentobarbital (Bimeda-MTC Animal Health Inc, Canada).

### Tissue fixation and processing

Two different protocols were used to fix the aorta in situ. In the first protocol (control n=3; experimental n=3), the abdominal aorta of the rabbit was rapidly exposed following sacrifice. The aorta was fixed in situ by adding 4% glutaraldehyde (BDH Inc, Canada) in 0.1 M

cacodylate buffer (Canemco Inc, Canada) (pH 7.4) into the abdominal cavity of the rabbit for 10 min. The abdominal aorta was then excised and immersion fixed with 2% glutaraldehyde in 0.1 M cacodylate buffer for 90 min. In the second protocol (control n=5; experimental n=5), the aorta was flushed with Krebs buffer in situ and perfusion fixed with 2% glutaraldehyde in 0.1 M cacodylate buffer at 100 cm of water pressure. The perfusion solutions were infused through the right carotid artery, down the aorta and drained from the inferior vena cava to perfuse the abdominal aorta in the direction of blood flow (38). The abdominal aorta was removed and immersion fixed with 2% glutaraldehyde in 0.1 M cacodylate buffer for 90 min. The second perfusion protocol was done to permit scanning electron microscopic observations of aortic surfaces. No difference in the quality of fixation was observed between these two protocols. All segments of the aorta that were harvested were processed and analyzed in the present study.

Following immersion fixation, segments of the aorta were randomly chosen for scanning electron microscopy (SEM) and transmission electron microscopy (TEM). Aortas destined for SEM were cut along the longitudinal axis resulting in two C-shaped pieces of aorta that varied in length from 0.5 cm to 2.0 cm. Aortas destined for TEM were cut into rings approximately 3 mm in width. Each ring was then turned onto its cut edge and cut into four to six small pieces suitable for TEM. All samples were then processed using standard electron microscopy processing (38,39). In brief, the samples were rinsed with 0.1 M cacodylate buffer and postfixed for 1 h in a solution of 1% OsO<sub>4</sub> (Marivic Inc, Canada) and 1% potassium ferrocyanide (Fisher Scientific Co, USA) in 0.1 M cacodylate buffer. Samples were rinsed with distilled water before graded acetone dehydration.

Samples for light microscopy (LM) and TEM were infiltrated with Epon 812 resin (Electron Microscopy Sciences, USA), and oriented so that sectioned tissues were viewed in the vessel cross-section (oriented 90° to the direction of blood flow) and polymerized overnight at 65°C. Blocks were trimmed and sectioned on a Leica EMUC6 Ultramicrotome (Leica Microsystems, Canada). LM sections (0.5 µm) were mounted on glass slides, stained with toluidine blue O and examined with a Nikon Labophot-2 Light Microscope (Nikon Canada Inc). Thin TEM sections (60 nm to 80 nm) were picked up on formvar-coated slot grids, stained with uranyl acetate and lead citrate, and then imaged using a Tecnai 12 TEM (FEI Company, USA) (38,39).

The following inclusion criteria were used in sample selection for histological analysis of the atherosclerotic plaques: the plaque thickness was greater than 100 µm; and if a plaque shoulder was present, sampling began 250 µm from the shoulder edge (measured along the internal elastic lamina).

### LM

The mean diameter of 75 randomly selected macrophage-derived foam cell profiles observed in section was used to establish a depth of interest 23 µm below the endothelium, where foam cells were close enough to interact with the endothelium and its immediate extracellular matrix (ECM) substrate. If more than 50% of a foam cell profile was within this depth of interest, it was counted as a subendothelial cell. Subendothelial macrophage profiles were counted on 0.5 µm sections cut from 88 different TEM blocks from the seven control rabbits and from 74 different TEM blocks from the five PM<sub>10</sub>-exposed rabbits. The unequal numbers of rabbits was due to an absence of atherosclerotic plaques in the region of the abdominal aortas of one control and three treated rabbits.

### Electron microscopy

All of the samples used for the LM analysis were also examined by TEM: images were captured in a systematic random fashion at ×9700 magnification. The first image was acquired two fields of view from the edge of the tissue section and five additional images were acquired, per block, from control and PM<sub>10</sub> blocks, with two fields of view separating each image.

Before morphometric analysis, the captured images were rotated in Photoshop (Adobe Systems Incorporated, USA) to orient the

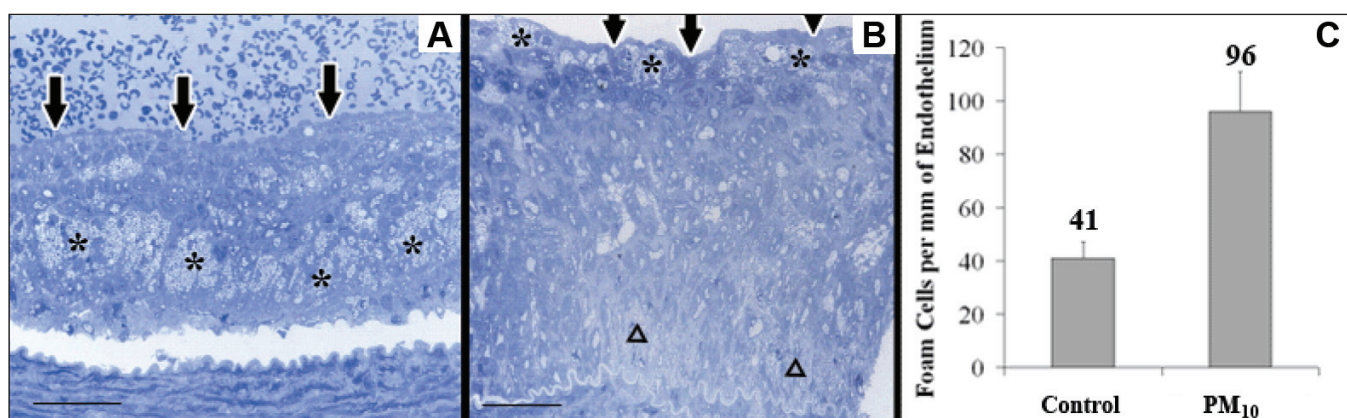


**Figure 1** **A** Macrophage-derived foam cells (\*) deep in the core of a control plaque. Below the intact endothelium (arrows) is a thick fibrous cap. The white space under the intima is a processing artifact. Scale bar = 50  $\mu$ m. **B** Accumulation of macrophage-derived foam cells (\*) at the abluminal surface of the intact endothelium (arrows) over a necrotic centre of gruel ( $\Delta$ ) in a particulate air pollution (particles smaller than 10  $\mu$ m in diameter; PM<sub>10</sub>)-exposed rabbit. Scale bar = 50  $\mu$ m. **C** Macrophage-derived foam cell population in the subendothelial region (mean  $\pm$  95% CI);  $P < 0.05$

endothelium horizontally. A cycloid grid mask was placed over the reoriented images parallel to the endothelium, and the line-intercept method (40,41) was used to quantify the frequency of endothelial contacts (15 nm or greater separation) with dense ECM, fragmented ECM, macrophages, macrophage-derived foam cells, SMCs, smooth muscle foam cells, unknown structures and space (an absence of electron-dense material).

Eight serial reconstructions were completed of the reticulum of dense ECM subtending the endothelium on the images obtained from four control and four PM<sub>10</sub>-exposed rabbits. Each reconstruction consisted of approximately 20 consecutive 100 nm thick sections of an atherosclerotic plaque. These images were captured at  $\times 37,000$  magnification, and then manually aligned and traced in Photoshop before application of three-dimensional reconstruction software (T3D, Research Systems Inc, USA). A similar protocol has been used previously to reconstruct the alveolar wall (42).

**SEM:** These samples were chemically dried using hexamethyldisilazane (Sigma-Aldrich Inc, USA) in a BioWave Microwave (Pelco International, USA) (43). After mounting dried specimens on aluminum stubs using adhesive spots, all samples were sputter coated with a gold/palladium alloy in a Nanotech SEM-Prep II Sputter Coater (Nanotech, United Kingdom). Samples were viewed using a Hitachi S4700 Field Emission Gun SEM (Hitachi, Canada). Sputter coating and SEM imaging were performed at the University of British Columbia Biomaging Facility (Vancouver).

#### Immunohistochemistry

WHHL rabbit aortic tissues that had undergone formalin fixation and paraffin embedding were immunostained for type IV collagen using the M3F7 antibody (University of Iowa, Hybridoma Bank, Iowa, USA) at 1/200 dilution. Slides were treated with pepsin in 0.5 N glacial acetic acid at 37°C for 3 h before a standard alkaline phosphatase method with Naphthol AS-BI phosphate (Sigma-Aldrich Inc) and New Fuchsin (Sigma-Aldrich Inc) substrate. To increase staining intensity, the secondary and tertiary antibody staining was repeated for 20 min. Positive and negative controls were included in each staining experiment. All slides were examined using a Nikon Labophot-2 Light Microscope and photographed on the Nikon Eclipse 50i.

#### Statistical analysis

To take into account the multiple samples from multiple rabbits, a nested ANOVA was performed for the analysis of the number of foam cells. Poisson regression analysis was used to analyze the data concerning abluminal endothelial contacts. All values were expressed as mean  $\pm$  SE, with  $P < 0.05$  considered to be significant.

## RESULTS

Qualitative LM observations made blinded to the exposure protocol showed that in the control rabbits, the atherosclerotic plaques had a stratified appearance; lipids were sequestered within macrophage-derived foam cells deep in the plaque cores with a dense layer of SMCs and ECM between the lipid core and the endothelial surface (Figure 1A). In contrast, plaque cores of PM<sub>10</sub>-exposed rabbits were composed mostly of extracellular lipid with an apparent accumulation of macrophage-derived foam cells immediately below the endothelium (Figure 1B).

The number of profiles of macrophage-derived foam cells found within the 23  $\mu$ m depth of interest was significantly greater ( $P = 0.04$ ) in the PM<sub>10</sub>-exposed rabbits compared with controls (Figure 1C, 96 cells/mm of endothelial length [95% CI 80 cells/mm to 110 cells/mm] versus 41 cells/mm of endothelial length [95% CI 35 cells/mm to 48 cells/mm]). These data suggested that macrophage-derived foam cells were accumulating under the endothelium of plaques from PM<sub>10</sub>-exposed rabbits.

TEM analysis of control atherosclerotic plaques revealed a reticulum of dense ECM subtending the endothelium (Figures 2A and 2B), SMCs with small cytoplasmic lipid accumulations and attendant basal laminae (Figure 2B), and only occasional macrophage-derived foam cells. The macrophage-derived foam cells were usually separated from the endothelial surface by the reticulum of dense ECM and showed very little lipid accumulation within the cells (Figure 2C). The analysis of the plaques from PM<sub>10</sub>-exposed rabbits revealed fragmentation or an absence of the reticulum of dense ECM in areas of macrophage-derived foam cell accumulation beneath the endothelium (Figures 2D and 2E). Observed within the macrophage-derived foam cells subtending the endothelium were large lipid deposits and frequent cholesterol crystals (Figure 2F). In adjacent regions without macrophage-derived foam cell accumulation, combinations of dense ECM and fragmented ECM were observed.

Line-intercept analysis of endothelial substrate contacts showed that 66% of the 2791 endothelial intersections in the control rabbits were in contact with elements of the reticulum of dense ECM compared with only 21% of the 3297 intersects in the PM<sub>10</sub>-exposed rabbits ( $P < 0.0001$ ; Figure 3). Furthermore, 22% of endothelial cell contacts were with fragments of the reticulum ECM in the PM<sub>10</sub>-exposed rabbits, compared with 8% of the contacts in control rabbits ( $P < 0.0001$ ). The number of endothelial cell contacts with macrophage-derived foam cells increased from 13% in the controls to 38% in the PM<sub>10</sub>-exposed rabbits ( $P = 0.0039$ ). Finally, the number of endothelial cell contacts with apparent space (an absence of electron-dense material) was 8% in controls and 14% in experimental rabbits ( $P < 0.0001$ ). The frequency of contact between endothelial cells and macrophages,

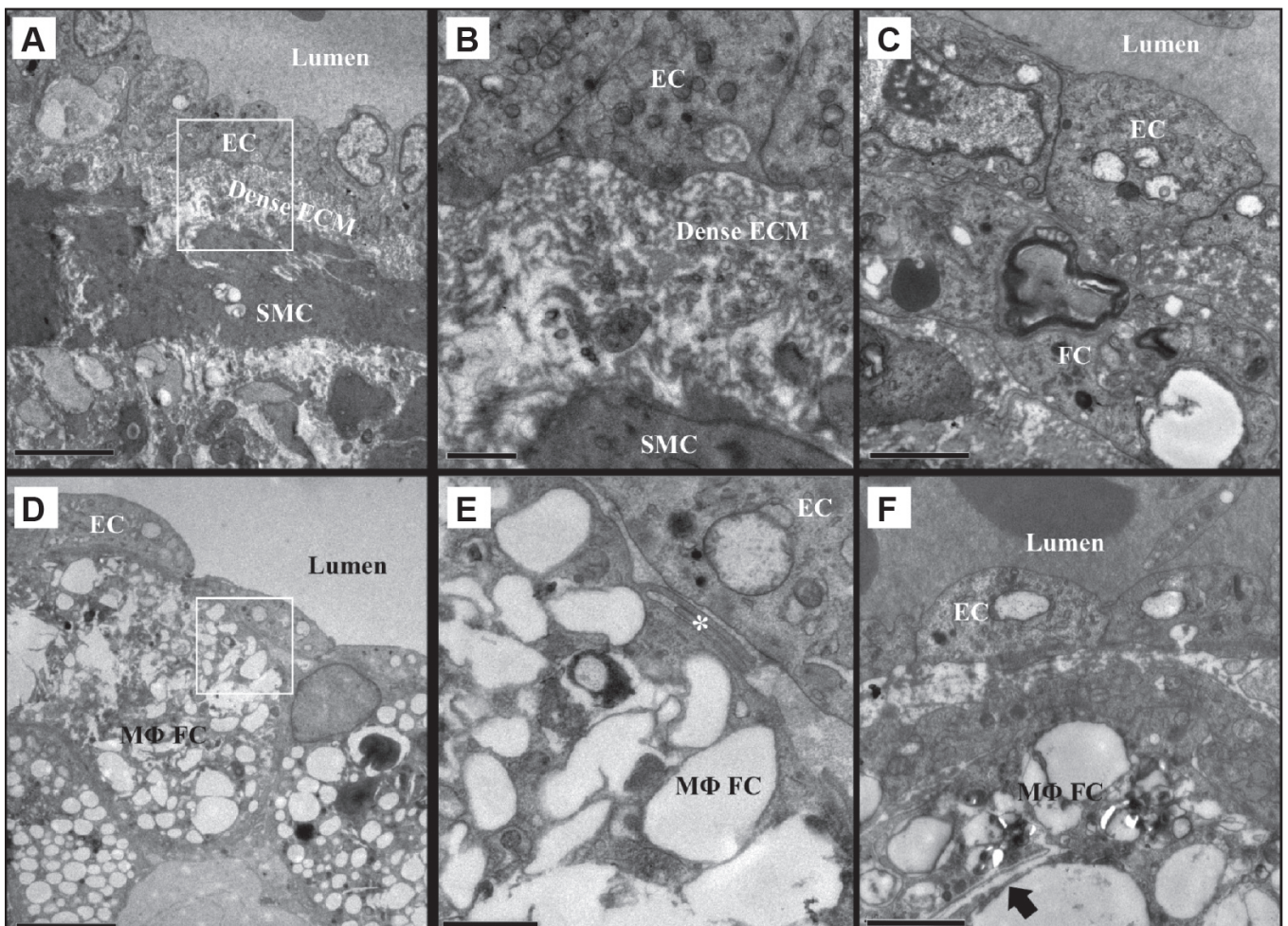


**Figure 2)** Subendothelial fibrous cap ultrastructure of Watanabe heritable hyperlipidemic rabbit atherosclerotic plaques. **A** Control rabbit endothelial cells (ECs) rest on a reticulum of dense extracellular matrix (ECM) subtended by smooth muscle cells (SMCs) and their ECM. **B** Reticulum of dense ECM and extracellular lipid droplets from **A**. **C** A foam cell (FC) with minimal lipid deposits located below the endothelium. There is a small area of contact between the FC and the EC. **D** Macrophage-derived FCs (MΦFCs) subtending the ECs in particulate air pollution (particles smaller than 10 μm in diameter)-exposed rabbits. **E** Reticulum of dense ECM is absent, leaving the MΦFCs in contact with the ECs (\*). **F** An MΦFC in close proximity to the endothelium loaded with large lipid deposits including a cholesterol crystal (arrow). **A** and **D** scale bar = 5 μm; **B** and **E** scale bar = 1 μm; **C** and **F** scale bar = 2 μm

SMCs, smooth muscle-derived foam cells and unknown structures was small with no measurable differences between control and experimental groups.

The three-dimensional reconstructions confirmed that the dense ECM subtending the endothelium in the plaques from control rabbits formed a reticulum of basal lamina-like material (Figure 4A). In addition, topographically, the reconstructed ECM closely matched the topography of the endothelial cells such that the shape and surface features of the endothelial cells were clearly reflected in the surface of the reticulum of dense ECM (Figures 4B and 4C). In contrast, in the reconstructions from PM<sub>10</sub>-exposed rabbits, the endothelium was subtended by small islands of the electron-dense ECM (Figure 4D). When the endothelial cell was electronically subtracted from these reconstructions, the ECM subtending the endothelium in the PM<sub>10</sub> reconstructions did not closely reflect the abluminal surface topography of the endothelial cells (Figures 4E and 4F).

Immunohistochemistry verified that the ECM material subtending the endothelium and surrounding SMCs contained type IV collagen – a molecular species usually confined to the basal lamina (Figure 5).

**SEM**

The luminal surface of the arterial wall revealed endothelium elongated along the axis of flow in nondiseased areas of both the control (Figure 6A) and the PM<sub>10</sub>-exposed (Figure 7A) rabbits. Flat

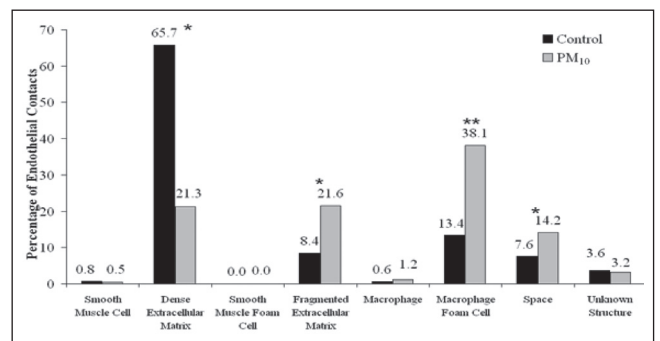


**Figure 3)** Relative percentage of endothelial cell abluminal membrane contacts (15 nm or less) with subtending cells or substrate elements. Particulate air pollution (particles smaller than 10 μm in diameter; PM<sub>10</sub>)-exposed rabbits (n=5) have significantly less contact with dense extracellular matrix, and significantly more contact with fragmented extracellular matrix, macrophage-derived foam cells and space than control rabbits (n=7). \*P<0.0001; \*\*P<0.005

interdigitating cytoplasmic extensions reached over the surface of neighbouring cells, creating an irregular border at endothelial cell margins. The atherosclerotic plaques in both experimental and

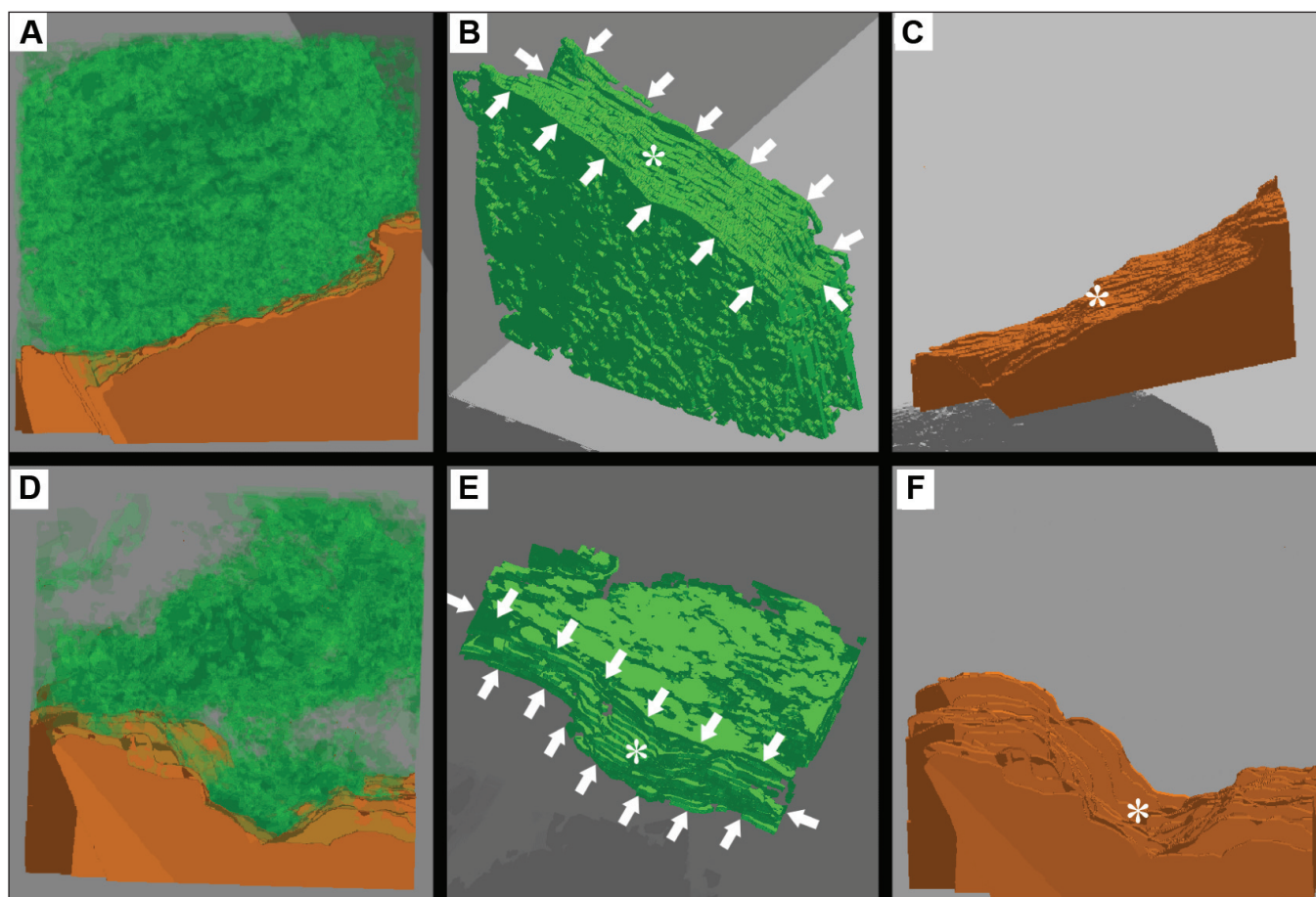


**Figure 4)** Serial section three-dimensional reconstructions of reticulum of dense extracellular matrix (ECM), magnification  $\times 37,000$ . Green indicates dense ECM; Orange indicates endothelial cells (EC). **A to C** Control reconstruction. **B** Surface of the ECM on which the EC rests (white arrows) closely reflects topography of the EC (\*). **C** Abluminal EC surface with ridge (\*) that is reflected in dense ECM. **D to F** Particulate air pollution (particles smaller than  $10\ \mu\text{m}$  in diameter) reconstruction. **E** The ECM surface on which the EC rests (white arrows) has holes and only reflects large surface features of the EC topography (\*). **F** The abluminal EC surface with the large dip (\*) that is reflected in dense ECM

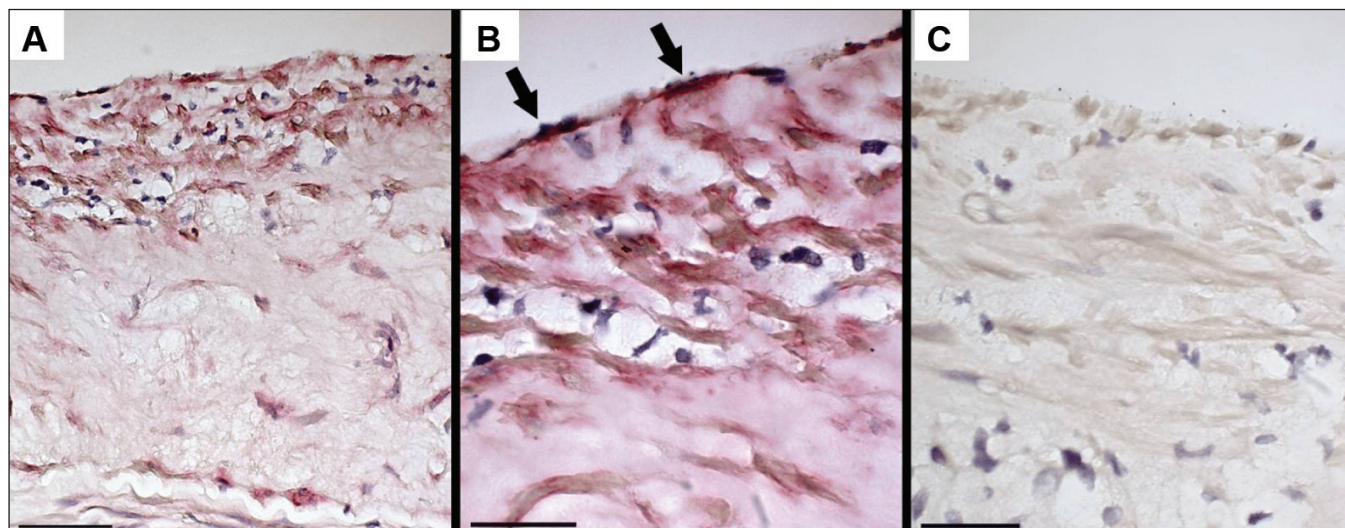


**Figure 5)** Immunostaining of control atherosclerotic plaques for type IV collagen. **A** Low magnification shows staining in the upper regions of the plaque; scale bar =  $50\ \mu\text{m}$ . **B** High magnification shows staining for type IV collagen (arrows) in the material subtending the endothelium; scale bar =  $25\ \mu\text{m}$ . **C** Immunoglobulin G control; scale bar =  $25\ \mu\text{m}$

control groups were easily identified by their elevated surfaces and sloping shoulders (Figure 6B). Endothelial topography over the core regions of control rabbit atherosclerotic plaques was more irregular than areas of endothelium from the nondiseased arterial

wall (Figures 6C and 6D), giving the surface of control atherosclerotic plaques an uneven appearance (Figures 6C and 6E). On the shoulder regions of the control atherosclerotic plaques, adherent and transmigrating leukocytes were observed (Figure 6F).

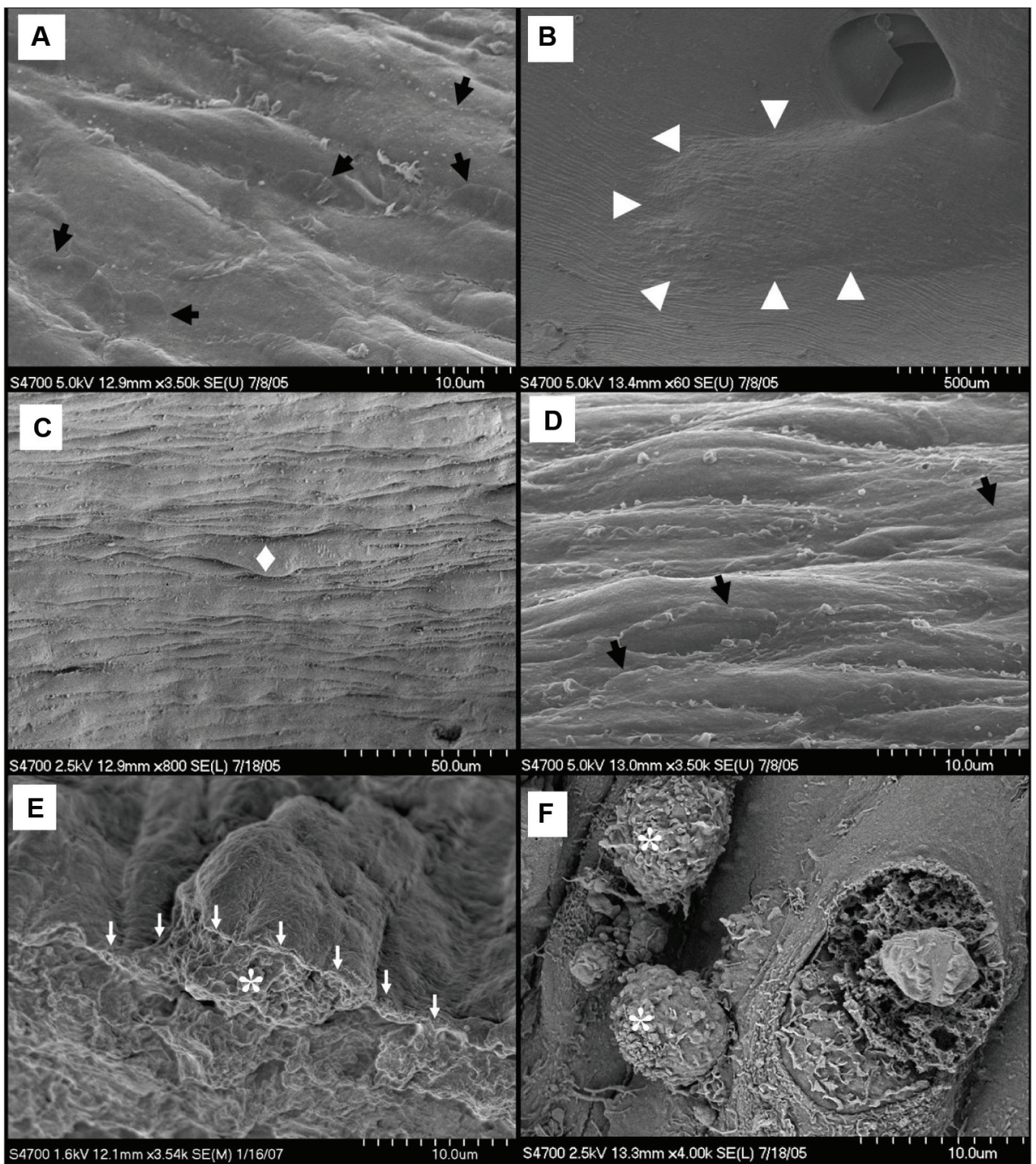


**Figure 6)** Atherosclerotic plaque topography from control Watanabe heritable hyperlipidemic rabbits. **A** Nonplaque endothelial cells with overlapping cytoplasmic flaps (arrows). **B** Plaque at a bifurcation (arrowheads). **C** Occasional endothelial protrusions (♦) making for irregular core topography. **D** Intact core endothelium with cytoplasmic flaps (arrows). **E** Macrophage-derived foam cell (\*) beneath protruding endothelium (arrows). **F** Two leukocytes (\*) on the plaque shoulder

Atherosclerotic plaques from PM<sub>10</sub>-exposed rabbits revealed small areas of endothelial desquamation to which platelets with signs of activation (ie, flat cells with long, thin cellular extensions) had adhered (Figure 7B). The endothelium at the sloping-shoulder regions was topographically irregular with adherent amoeboid leukocytes

(Figures 7C and 7D). In addition, clusters of large leukocytes were observed on the endothelium at locations strongly suggesting both transcellular (Figures 8A and 8B) and paracellular (Figures 8C and 8D) leukocyte transmigration across the endothelium, over the plaque surfaces as well as at the plaque shoulders of PM<sub>10</sub>-exposed

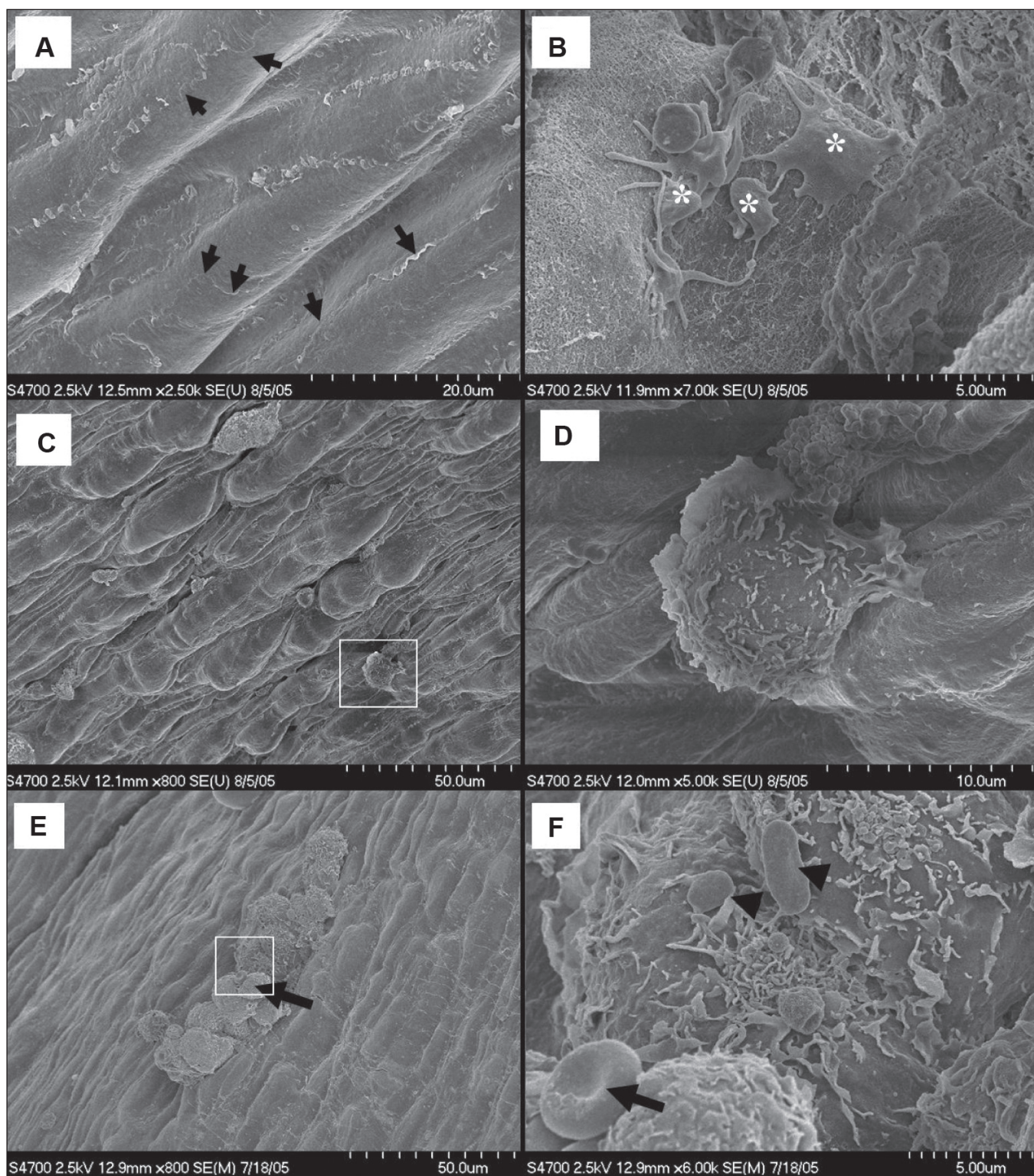


**Figure 7)** Atherosclerotic plaque topography from particulate air pollution (particles smaller than 10  $\mu\text{m}$  in diameter;  $\text{PM}_{10}$ )-exposed Watanabe heritable hyperlipidemic rabbits. **A** Nondiseased regions with interdigitating overlapping flaps (arrows). **B** Endothelial erosion with spreading activated platelets (\*). **C** Irregular topography of the plaque shoulder with adherent leukocytes. **D** (Inset from **C**) The polarized adherent amoeboid leukocyte with anterior lamellipodial front and trailing uropod. **E** A leukocyte cluster over the core of an atherosclerotic plaque from a  $\text{PM}_{10}$ -exposed rabbit. **F** (Inset from **E**) Red blood cells (arrow) and platelets (arrowheads) attached to leukocytes

rabbits. These leukocytes had numerous cytoplasmic flaps and bore occasional adherent round or oval (unactivated) platelets (Figure 7F). Endothelial filopodia extended up the sides of the transminating cells to terminate at apparent focal adhesions (Figures 8B and 8D).

TEM of protruding cells revealed that they were macrophage-derived foam cells (Figure 9) – some of which carried isolated segments of dense ECM reticulum in pockets on their surfaces (Figures 9B and 9C). The gap in the arterial endothelium through which this foam cell

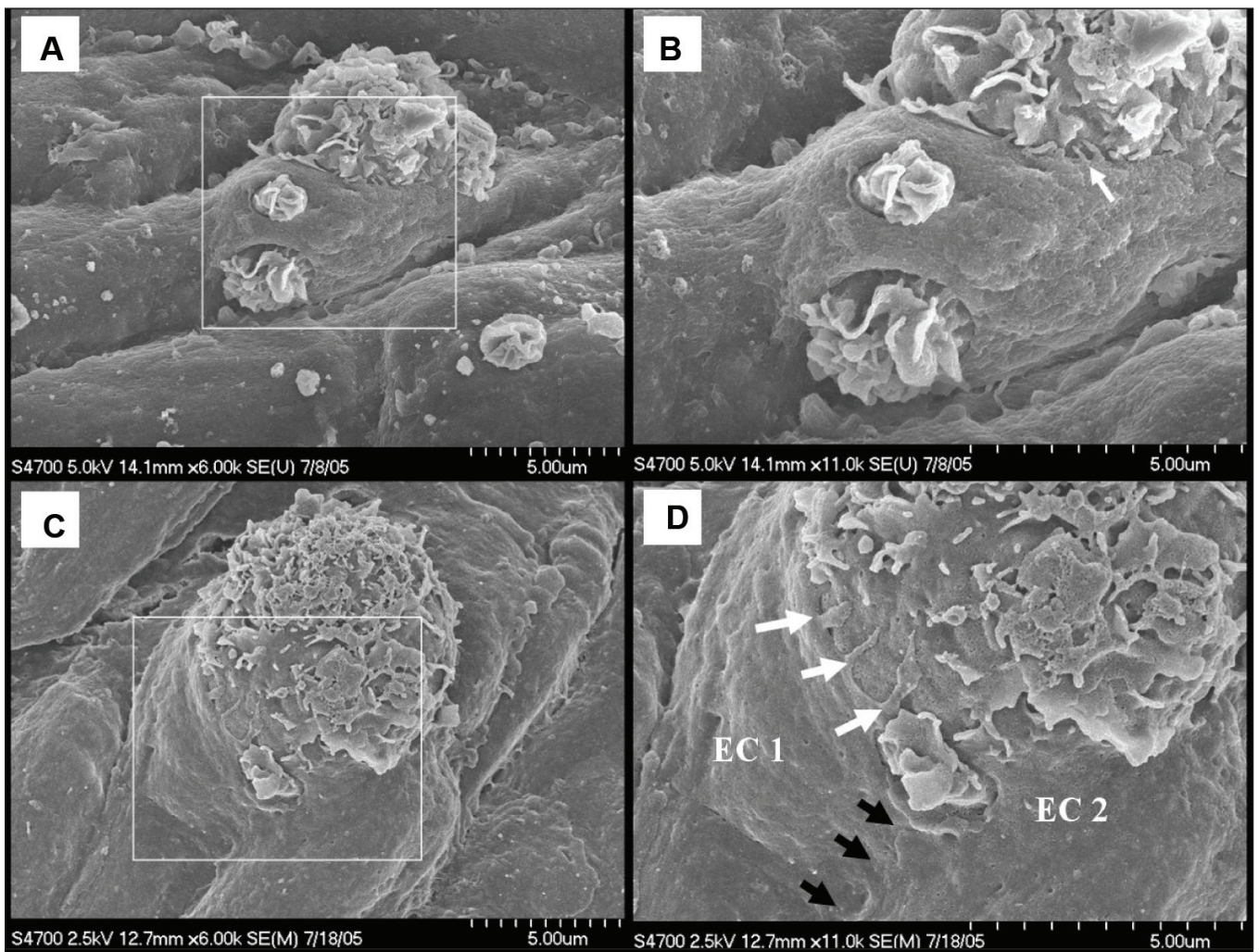


**Figure 8)** Protruding leukocytes on the surface of plaques from particulate air pollution (particles smaller than 10 µm in diameter)-exposed rabbits. **A** Leukocyte protruding through apertures in the endothelium. **B** (Inset from **A**) Small endothelial filopodia extending up the side of the protruding cell (arrow). **C** Another migrating leukocyte with nonpolarized lamellipodia. **D** (Inset from **C**) Paracellular migration at a bicellular junction (black arrows) with three filopodia of endothelial cell (EC) 1 extending up the leukocyte (white arrows)

extended into the vascular lumen is not a mechanical artifact because it is delineated by intact plasma membrane (Figure 9C).

### DISCUSSION

The observations presented herein show that macrophage-derived foam cells occur in differing areas in the atherosclerotic plaques from WHHL rabbits that received repeated instillations of PM<sub>10</sub> in the lungs, compared with the control rabbits. A complete analysis of our data derived from multiple types of microscopy led us to the unexpected conclusion that macrophage-derived foam cells emigrate from the centres of the atherosclerotic plaque into the circulation. In this process of macrophage-derived foam cell emigration, the observational data suggest that the endothelial cell to substrate contact was reduced through a combination of physical separation from and fragmentation of the subendothelial reticulum of dense ECM. Endothelial separation from its substrate and the emigration of macrophage-derived foam cells may compromise normal endothelial function and contribute to plaque instability.

The data that led to this conclusion can be separated into three observations. The first observation is the presence of macrophage-derived foam cells in the subendothelial region. The morphometric analysis of the subendothelial contacts revealed a 25% increase (from 13% to 38%) in the contacts between macrophage-derived foam cells in PM<sub>10</sub>-exposed rabbits compared

with control rabbits. TEM analysis further revealed the presence of cholesterol crystals in the macrophage-derived foam cells in the region immediately below the endothelium of the PM<sub>10</sub>-exposed rabbits. By comparison, in the control rabbits, cholesterol crystals were only found in macrophage-derived foam cells deep within the cores of atherosclerotic plaques. We suggest that the lipid-filled macrophage-derived foam cells immediately below the endothelium of PM<sub>10</sub>-exposed rabbits originated in and migrated from the cores of these plaques, rather than having developed from recently immigrated monocytes. The frequency of this observation and the presence of cholesterol crystals within the cells supports this suggestion.

The second observation is the altered ECM subtending the endothelial cells. Without an ECM foundation, the stability and integrity of the endothelial layer are compromised, resulting in this layer becoming a contributor to atherosclerotic plaque instability, and a possible precursor to plaque rupture and acute cardiovascular events (44,45). The reticulum of dense ECM elements observed within the plaques is structurally similar to that reported by Nakamura et al (46) in aging rats and differs from the normal basal lamina found in nondiseased arteries. Type IV collagen is typically located within the endothelial basal lamina in healthy blood vessel walls (47). The presence of type IV collagen in the dense ECM subtending the endothelium suggests that the observed thickened reticulum subtending the plaque endothelial cells is a modified form



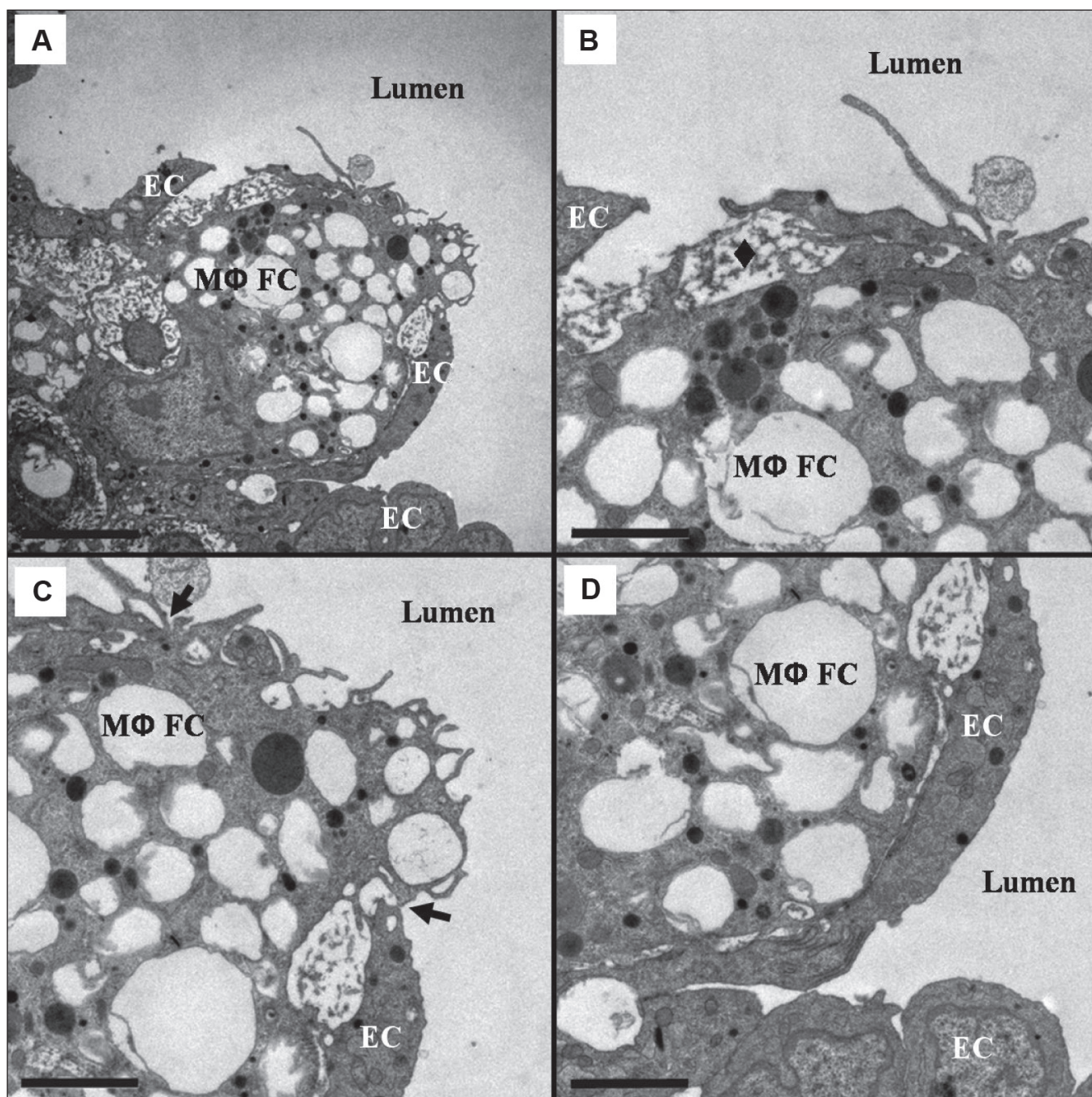


**Figure 9** **A** Protruding leukocyte is a macrophage-derived foam cell (MΦFC). **B** MΦFC carrying segments of reticulum of dense extracellular matrix in surface cavities (◆). **C** Lamellipodia-covered MΦFC protruding through endothelial aperture (between arrows). MΦFC surface cavity contains segments of reticulum of dense extracellular matrix that has been fragmented. **D** MΦFC protrusion has doubled the endothelium back onto itself into the lumen. **A** Scale bar = 5  $\mu\text{m}$ ; **B** to **D** Scale bar = 2  $\mu\text{m}$ . EC Endothelial cell

of the endothelial basal lamina. The three-dimensional reconstructions performed on the serial electron microscopic sections of plaques confirmed that the subendothelial matrix was a porous reticulum. When the endothelium was electronically subtracted from the reconstructed underlying matrix in the control rabbits, the surface topography of the matrix closely reflected the shape of the endothelial cells, verifying apposition of these two surfaces. In contrast, subtraction of the endothelial layer from the underlying matrix in the PM<sub>10</sub>-exposed rabbits showed no reflection of the shape, size or surface topography of the endothelium, suggesting a loss of contact and, presumably, adhesion.

Due to the labour-intensive nature of serial reconstructions and the small sample area, the line-intercept technique was used to increase the sample size for analysis of the endothelial cell/ECM contact surface area. The line-intercept morphometric analysis confirmed that the reticulum of dense ECM was fragmented in the PM<sub>10</sub>-exposed rabbits. Macrophages release matrix metalloproteinases (MMPs) that can degrade the ECM (48) and, although we were unable to determine the MMPs in the tissue due to the glutaraldehyde fixation protocol used, we hypothesized that MMPs secreted by the migrating macrophage-derived foam cells that accumulated under the endothelium could be responsible for the observed

ECM degradation. Several studies in the ApoE<sup>-/-</sup> mouse have shown the transcriptional upregulation of factors associated with vascular remodelling including MMP-3, -7 and -9 following PM<sub>10</sub> exposure (29,30), and MMP-9 following diesel exhaust exposure (31). Future work testing for colocalization of these MMPs with migrating foam cells in the WHHL rabbit model would be of interest.

The third and final observation was that while monocytes were observed apparently immigrating at plaque margins, macrophage-derived foam cells were observed emigrating from the core regions of atherosclerotic plaques of PM<sub>10</sub>-exposed rabbits. The immigration of monocytes as observed by SEM along the plaque shoulders has been previously reported in atherosclerotic disease (49). In addition, increased recruitment of monocytes throughout the entire depth of atherosclerotic plaques from WHHL rabbits exposed to PM<sub>10</sub> (32) and increased trends in macrophage accumulation in atherosclerotic plaques from ApoE<sup>-/-</sup> mice following diesel emission exposure (31) have been reported. The observations presented here of adherent cells over the shoulder regions of the atherosclerotic plaques and over the core regions of the atherosclerotic plaques in PM<sub>10</sub>-exposed rabbits is in agreement with these previous reports. However, the observation of macrophage-derived foam cell emigration out of the core regions of the atherosclerotic plaques was unexpected. The observations supporting the conclusion of emigration were the endothelial filopodia extending from the endothelial cell edges to terminate at focal adhesions up on the luminal surface of macrophage-derived foam cells; and the discovery of segments of fragmented reticulum of dense ECM in pockets of the luminal surface of macrophage-derived foam cells. The latter observation suggests that the cells were actually carrying components of the ECM as they emerged into the vascular lumen (Figures 4B and 4C). Gerrity (50) used SEM to show large macrophage-derived foam cells distending the endothelial surface and hypothesized that the cells were emigrating in an attempt to clear accumulated lipid from atherosclerotic plaques; however, no electron microscopic images of migration were published.

When taken together, these three observations support macrophage-derived foam cell transmigration in response to the deposition of PM<sub>10</sub> in the lungs. This suggests that particle deposition is causally associated with the remodelling of existing atherosclerotic plaques. If intrapulmonary particle deposition is causally related to transmigration and remodelling of plaques, then the protocol for particle delivery is relevant. Ideally, to truly mimic airway dosage and deposition location, these rabbits would have been exposed to PM<sub>10</sub> by inhalation rather than intratracheal deposition. In choosing the animal model, we tried to avoid an atherosclerotic model that required cholesterol feeding (the ApoE<sup>-/-</sup> mouse). However, because the WHHL rabbit is an obligate nose-breathing animal, satisfactory airborne inhalation exposures are almost impossible to achieve. Previous work with the WHHL rabbits has estimated that only 20% of the 5 mg of PM<sub>10</sub> deposited just above the larynx of the rabbit using our protocol is aspirated into the lungs, and only 4% reaches the alveolar surface (36). With an estimated 5.9 m<sup>2</sup> alveolar surface for a 2.5 kg rabbit, the calculated alveolar exposure was 4.3 ng/cm<sup>2</sup> for each dose or 34.4 ng/cm<sup>2</sup> over the experimental period. This exposure is similar to a human exposed to 150 µg/m<sup>3</sup> for 20 days. The authors acknowledge that while these exposure levels are considered to be high, they are still biologically relevant exposure levels (eg, the exposure of humans during the Southeast Asian forest fires of 1997 [51]). We also acknowledge that this delivery mechanism results in high sporadic doses compared with continuous inhalation from the environment; however, epidemiologically, the connection between PM<sub>10</sub> exposure and increased cardiovascular morbidity and mortality resulted from sporadic increases in human exposure to PM<sub>10</sub>. Therefore, we believe that these observations are relevant to the further understanding of how PM<sub>10</sub> exposure leads to cardiovascular morbidity and mortality. These experimental challenges suggest that it would

be of interest to develop an inhalation model using the WHHL rabbit in the future.

Our laboratory has previously shown that when particles are deposited in the lung using this instillation protocol, a rapid release of polymorphonuclear leukocytes (26) and monocytes (20) into the circulation from the bone marrow is induced. Furthermore, this response is proportional to the amount of particulate matter phagocytosed by alveolar macrophages (20). It has also been observed that lung instillation of supernatants from alveolar macrophages exposed to these particles *in vitro* has a similar effect (37). Other studies indicate that interactions between macrophages and lung epithelial cells enhance the *in vitro* release of a wide variety of cytokines including tumour necrosis factor- $\alpha$ , IL-1, granulocyte-macrophage colony-stimulating factor, IL-6 and IL-8 – all of which are involved in the acute-phase systemic inflammatory response (52). For a more detailed discussion of the pulmonary and systemic response to PM<sub>10</sub> exposure, please refer to a recent review by Hogg and van Eeden (53). Our working hypothesis is that the cytokines released into the circulation lead to a systemic inflammatory response that follows PM<sub>10</sub> exposure (51) and activates the endothelium covering the atherosclerotic plaques (32). This endothelial activation could result in the release of the chemotactic stimuli responsible for the emigration of macrophage-derived foam cells from plaque cores, through the fibrous cap, across the endothelium and onto the lumen of the aorta. Validation of this hypothesis may shed light on the process of atherosclerotic plaque remodelling including lipid redistribution and fibrous cap thinning.

The clinical implication of our observations is a greater understanding of how and why atherosclerotic plaques may become destabilized following exposure to particulate matter air pollution. The authors speculate that air pollution exposure exacerbates existing disease; however, the authors further speculate that risk factors such as obesity, smoking and a sessile lifestyle probably contribute to atherosclerotic plaque development to a greater extent than air pollution exposure.

The model used for the present work is the homozygotic WHHL rabbit. WHHL rabbits have a spontaneous four amino acid deletion in the cysteine-rich ligand-binding domain of the low-density lipoprotein (LDL) receptor gene – the same gene associated with human familial hypercholesterolemia (54-56). In both humans and rabbits, this genetic defect produces a drastic reduction of plasma membrane LDL receptors on endothelial cells and leads to the decreased clearance of lipoproteins, resulting in extremely high levels of LDL in the circulating blood (55,57). In the WHHL rabbit, which has both hypercholesterolemia and hypertriglyceridemia (56), atherosclerosis typically develops without the need for cholesterol feeding by five months of age, and progresses in both severity and extent of disease as the animal ages (57). Compared with atherosclerotic animal models that require cholesterol feeding for atherosclerotic plaque development, the WHHL homozygotic rabbit model develops atherosclerotic plaques on a normal diet and the plaques are indistinguishable from human atherosclerotic plaques (57). Although this model has a genetic defect that affects one in 500 people, it appears to be a very good model to study the etiology of atherosclerosis and how air pollution may alter the ultrastructure of existing atherosclerotic plaques. However, one challenge associated with the inbred WHHL rabbit model is the inconsistency of plaque formation compared with knockout models such as the ApoE<sup>-/-</sup> mouse. Furthermore, of the regions of the aorta, the thoracic aorta is more prone to atherosclerotic plaque formation than the abdominal aorta (56). However, because of the need to accommodate multiple investigators, sampling for the present study was confined to the abdominal aorta of the WHHL rabbits to maximize tissue sample availability. Our finding of variable plaque formation in the abdominal aortas of WHHL rabbits is not surprising given previous observations in the literature and does not preclude plaque existence in the thoracic aortas (56). Future studies could focus on the thoracic aorta to maximize the availability of

atherosclerotic plaques for investigation and to extend our observations to the typically more diseased aortic segment.

## CONCLUSION

Following PM<sub>10</sub> deposition into the lungs of the WHHL rabbit, we have quantitatively demonstrated architectural changes in atherosclerotic plaques that are consistent with the phenotypic characteristics of unstable atherosclerotic plaques. We have further provided evidence of the emigration of macrophage-derived foam cells from the atherosclerotic plaques back into circulation. Given the existing literature on macrophage-derived foam cells, we speculate that migrating foam cells could be responsible for the remodelling of the atherosclerotic

plaques following exposure to particulate matter air pollution in ways that could contribute to plaque instability.

**ACKNOWLEDGEMENTS:** The authors thank Renaud Vincent for the EHC-93 particles, Dean English and the late Stuart Greene for imaging expertise, Mark Elliott for assistance with the immunohistochemistry protocol and Alan Burns for reading the manuscript. Dr van Eeden is a Michael Smith Foundation for Health Research Senior Investigator.

**FUNDING:** This work was supported by the Heart and Stroke Foundation of Canada and the Canadian Institutes of Health Research.

## REFERENCES

- Dockery DW, Pope CA III, Xu X, et al. An association between air pollution and mortality in six U.S. cities. *N Engl J Med* 1993;329:1753-9.
- Samet JM, Dominici F, Currier FC, Coursac I, Zeger SL. Fine particulate air pollution and mortality in 20 U.S. cities, 1987-1994. *N Engl J Med* 2000;343:1742-9.
- Araujo JA, Barajas B, Kleinman M, et al. Ambient particulate pollutants in the ultrafine range promote early atherosclerosis and systemic oxidative stress. *Circ Res* 2008;102:589-96.
- Peters A, Dockery DW, Muller JE, Mittleman MA. Increased particulate air pollution and the triggering of myocardial infarction. *Circulation* 2001;103:2810-5.
- Pope CA III, Burnett RT, Thurston GD, et al. Cardiovascular mortality and long-term exposure to particulate air pollution: Epidemiological evidence of general pathophysiological pathways of disease. *Circulation* 2004;109:71-7.
- Berglund N, Bellander T, Forastiere F, et al. Ambient air pollution and daily mortality among survivors of myocardial infarction. *Epidemiology* 2009;20:110-8.
- Zanobetti A, Schwartz J. Are diabetics more susceptible to the health effects of airborne particles? *Am J Respir Crit Care Med* 2001;164:831-3.
- Pereira Filho MA, Pereira LA, Arbex FF, et al. Effect of air pollution on diabetes and cardiovascular diseases in Sao Paulo, Brazil. *Braz J Med Biol Res* 2008;41:526-32.
- Peters A, von Klot S, Heier M, et al. Exposure to traffic and the onset of myocardial infarction. *N Engl J Med* 2004;351:1721-30.
- Hong YC, Lee JT, Kim H, Kwon HJ. Air pollution: A new risk factor in ischemic stroke mortality. *Stroke* 2002;33:2165-9.
- Peters A, Liu E, Verrier RL, et al. Air pollution and incidence of cardiac arrhythmia. *Epidemiology* 2000;11:11-7.
- Schwartz J. What are people dying of on high air pollution days? *Environ Res* 1994;64:26-35.
- Ibald-Mulli A, Stieber J, Wichmann HE, Koenig W, Peters A. Effects of air pollution on blood pressure: A population-based approach. *Am J Public Health* 2001;91:571-7.
- Peters A, Doring A, Wichmann HE, Koenig W. Increased plasma viscosity during an air pollution episode: A link to mortality? *Lancet* 1997;349:1582-7.
- Brook RD, Brook JR, Urch B, et al. Inhalation of fine particulate air pollution and ozone causes acute arterial vasoconstriction in healthy adults. *Circulation* 2002;105:1534-6.
- Ulrich MM, Alink GM, Kumarathasan P, et al. Health effects and time course of particulate matter on the cardiopulmonary system in rats with lung inflammation. *J Toxicol Environ Health A* 2002;65:1571-95.
- Mutlu GM, Green D, Bellmeyer A, et al. Ambient particulate matter accelerates coagulation via an IL-6-dependent pathway. *J Clin Invest* 2007;117:2952-61.
- Nemmar A, Hoet PH, Dinsdale D, et al. Diesel exhaust particles in lung acutely enhance experimental peripheral thrombosis. *Circulation* 2003;107:1202-8.
- Mukae H, Hogg JC, English D, Vincent R, van Eeden SF. Phagocytosis of particulate air pollutants by human alveolar macrophages stimulates the bone marrow. *Am J Physiol Lung Cell Mol Physiol* 2000;279:L924-31.
- Goto Y, Hogg JC, Shih CH, et al. Exposure to ambient particles accelerates monocyte release from bone marrow in atherosclerotic rabbits. *Am J Physiol Lung Cell Mol Physiol* 2004;287:L79-85.
- Virmani R, Burke AP, Farb A, Kolodgie FD. Pathology of the vulnerable plaque. *J Am Coll Cardiol* 2006;47(8 Suppl):C13-8.
- Davies MJ, Richardson PD, Woolf N, Katz DR, Mann J. Risk of thrombosis in human atherosclerotic plaques: Role of extracellular lipid, macrophage, and smooth muscle cell content. *Br Heart J* 1993;69:377-81.
- Fuster V, Fayad ZA, Badimon JJ. Acute coronary syndromes: Biology. *Lancet* 1999;353(Suppl 2):S115-9.
- Shah PK. Pathophysiology of coronary thrombosis: Role of plaque rupture and plaque erosion. *Prog Cardiovasc Dis* 2002;44:357-68.
- Seaton A, Soutar A, Crawford V, et al. Particulate air pollution and the blood. *Thorax* 1999;54:1027-32.
- Suwa T, Hogg JC, Quinlan KB, et al. Particulate air pollution induces progression of atherosclerosis. *J Am Coll Cardiol* 2002;39:935-42.
- Sun Q, Wang A, Jin X, et al. Long-term air pollution exposure and acceleration of atherosclerosis and vascular inflammation in an animal model. *JAMA* 2005;294:3003-10.
- Sun Q, Yue P, Kirk RI, et al. Ambient air particulate matter exposure and tissue factor expression in atherosclerosis. *Inhal Toxicol* 2008;20:127-37.
- Lund AK, Knuckles TL, Obot Akata C, et al. Gasoline exhaust emissions induce vascular remodeling pathways involved in atherosclerosis. *Toxicol Sci* 2007;95:485-94.
- Lund AK, Lucero J, Lucas S, et al. Vehicular emissions induce vascular MMP-9 expression and activity associated with endothelin-1-mediated pathways. *Arterioscler Thromb Vasc Biol* 2009;29:511-7.
- Campen MJ, Lund AK, Knuckles TL, et al. Inhaled diesel emissions alter atherosclerotic plaque composition in ApoE(-/-) mice. *Toxicol Appl Pharmacol* 2010;242:310-7.
- Yatera K, Hsieh J, Hogg JC, et al. Particulate matter air pollution exposure promotes recruitment of monocytes into atherosclerotic plaques. *Am J Physiol Heart Circ Physiol* 2008;294:H944-53.
- Vincent R, Goegan P, Johnson G, et al. Regulation of promoter-CAT stress genes in HepG2 cells by suspensions of particles from ambient air. *Fundam Appl Toxicol* 1997;39:18-32.
- World Health Organization. WHO Air Quality Guidelines for Europe. Regional Office for Europe, Copenhagen: World Health Organization, 2000.
- Osornio-Vargas AR, Bonner JC, Alfaro-Moreno E, et al. Proinflammatory and cytotoxic effects of Mexico City air pollution particulate matter in vitro are dependent on particle size and composition. *Environ Health Perspect* 2003;111:1289-93.
- Mukae H, Vincent R, Quinlan K, et al. The effect of repeated exposure to particulate air pollution (PM10) on the bone marrow. *Am J Respir Crit Care Med* 2001;163:201-9.
- Goto Y, Ishii H, Hogg JC, et al. Particulate matter air pollution stimulates monocyte release from the bone marrow. *Am J Respir Crit Care Med* 2004;170:891-7.
- Hayat MA. Principles and Techniques of Electron Microscopy, 3rd edn. Boca Raton: CRC Press Inc, 1989:1-78.
- Robards AW, Wilson AJ, eds. Procedures in Electron Microscopy. New York: John Wiley & Sons Ltd, 1993.
- Howard CV, Reed MG. Unbiased Stereology: Three-Dimensional Measurement in Microscopy. New York: Springer-Verlag, 1998:25-29,33-36,109.

41. Weibel ER. *Stereological Methods: Volume 1. Practical Methods for Biological Morphometry*. London: Academic Press, 1979;9-60,116-123,372.
  42. Sirianni FE, Milaninezhad A, Chu FS, Walker DC. Alteration of fibroblast architecture and loss of basal lamina apertures in human emphysematous lung. *Am J Respir Crit Care Med* 2006;173:632-8.
  43. Humphrey E. Microwave processing in a modern microscopy facility. *Microsc Microanal* 2006;12(Supp 2):194-5.
  44. Libby P. Inflammation in atherosclerosis. *Nature* 2002;420:868-74.
  45. Newby AC, Zaltsman AB. Fibrous cap formation or destruction – the critical importance of vascular smooth muscle cell proliferation, migration and matrix formation. *Cardiovasc Res* 1999;41:345-60.
  46. Nakamura H, Izumiyama N, Nakamura K, Ohtsubo K. Age-associated ultrastructural changes in the aortic intima of rats with diet-induced hypercholesterolemia. *Atherosclerosis* 1989;79:101-11.
  47. Gelse K, Poschl E, Aigner T. Collagens – structure, function, and biosynthesis. *Adv Drug Deliv Rev* 2003;55:1531-46.
  48. Johnson JL. Matrix metalloproteinases: Influence on smooth muscle cells and atherosclerotic plaque stability. *Expert Rev Cardiovasc Ther* 2007;5:265-82.
  49. Walker LN, Reidy MA, Bowyer DE. Morphology and cell kinetics of fatty streak lesion formation in the hypercholesterolemic rabbit. *Am J Pathol* 1986;125:450-9.
  50. Gerrity RG. The role of the monocyte in atherogenesis: II. Migration of foam cells from atherosclerotic lesions. *Am J Pathol* 1981;103:191-200.
  51. van Eeden SF, Hogg JC. Systemic inflammatory response induced by particulate matter air pollution: The importance of bone-marrow stimulation. *J Toxicol Environ Health A* 2002;65:1597-613.
  52. Ishii H, Fujii T, Hogg JC, et al. Contribution of IL-1 beta and TNF-alpha to the initiation of the peripheral lung response to atmospheric particulates (PM10). *Am J Physiol Lung Cell Mol Physiol* 2004;287:L176-83.
  53. Hogg JC, van Eeden S. Pulmonary and systemic response to atmospheric pollution. *Respirology* 2009;14:336-46.
  54. Yamamoto T, Bishop RW, Brown MS, Goldstein JL, Russell DW. Deletion in cysteine-rich region of LDL receptor impedes transport to cell surface in WHHL rabbit. *Science* 1986;232:1230-7.
  55. Aliev G, Burnstock G. Watanabe rabbits with heritable hypercholesterolaemia: A model of atherosclerosis. *Histol Histopathol* 1998;13:797-817.
  56. Goldstein JL, Kita T, Brown MS. Defective lipoprotein receptors and atherosclerosis. Lessons from an animal counterpart of familial hypercholesterolemia. *N Engl J Med* 1983;309:288-96.
  57. Clubb FJ, Cerny JL, Deferrari DA, et al. Development of atherosclerotic plaque with endothelial disruption in Watanabe heritable hyperlipidemic rabbit aortas. *Cardiovasc Pathol* 2001;10:1-11.
-